IEEE Access
Multidisciplinary | Rapid Review | Open Access Journal

Received May 17, 2021, accepted June 2, 2021, date of publication June 14, 2021, date of current version June 23, 2021.

Digital Object Identifier 10.1109/ACCESS.2021.3089005

On the Queuing Delay of Time-Varying Channels in Low Earth Orbit Satellite Constellations

NÉSTOR J. HERNÁNDEZ MARCANO[1], (Member, IEEE), LUIS DIEZ[2], RAMÓN AGÜERO CALVO[2], (Senior Member, IEEE), AND RUNE HYLSBERG JACOBSEN[1], (Senior Member, IEEE)

[1]DIGIT, Department of Electrical and Computer Engineering, Aarhus University, 8200 Aarhus, Denmark
[2]Communications Engineering Department, Universidad de Cantabria, 39005 Santander, Spain

Corresponding author: Néstor J. Hernández Marcano (nh@ece.au.dk)

This work was supported in part by the European Union's Horizon 2020 Research and Innovation Programme under Grant 861111, in part by the Innovation Fund Denmark Project Drones4Energy under Project J.nr.8057-00038A, and in part by the Spanish Government through the Ministerio de Economía y Competitividad, Fondo Europeo de Desarrollo Regional (MINECO-FEDER) by the Project Future Internet Enabled Resilient smart CitiEs (FIERCE) under Grant RTI2018-093475-AI00.

ABSTRACT Low Earth Orbit (LEO) satellite constellations are envisioned as a complementary or integrated part of 5G and future 6G networks for broadband or massive access, given their capabilities of full Earth coverage in inaccessible or very isolated environments. Although the queuing and end-to-end delays of such networks have been analyzed for channels with fixed statistics, currently there is a lack in understanding the effects of more realistic time-varying channels for traffic aggregation across such networks. Therefore, in this work we propose a queuing model for LEO constellation-based networks that captures the inherent variability of realistic satellite channels, where ground-to-satellite/satellite-to-ground links may present extremely poor connection periods due to the Land Mobile Satellite (LMS) channel. We verify the validity of our model with an extensive event-driven simulator framework analysis capturing the characteristics of the considered scenario. We later study the queuing and end-to-end delay distributions under such channels with various link, traffic, packet and background conditions, while observing good match between theory and simulation. Our results show that ground-to-satellite/satellite-to-ground links and background traffic have a much stronger impact over the end-to-end delay in mean and particularly variance, even with moderate queues, than unobstructed inter-satellite connections in outer space on an established path between two ground stations and through the constellation. This might hinder the usability of these networks for services with stringent time requirements.

INDEX TERMS Queuing, delay, LEO, constellation, LMS channel, Internet of Things.

I. INTRODUCTION

In recent years, the reborn interest in commercial space applications from service providers and academia has led to the so-called NewSpace / Space 4.0 era [1]–[3]. It has been indeed publicly recognized in the National Aeronautics and Space Administration (NASA) new ARTEMIS program to the Moon, starting on 2022 [4]. To reach this end, rocket launchers as SpaceX or Blue Origin have introduced significant launch cost reductions for different missions types including LEO satellite constellations. This has been possible by leveraging on both reusable propulsion rockets [3], [5], [6], and small satellites from Commercial Off-the-Shelf (COTS) components [7], [8]. All of this has also been translated into technology transfer and low cost electronics for society.

The progressive acceptance of 5G New Radio (NR) by Third Generation Partnership Project (3GPP) and the Internet of Things (IoT) is enabling mobile operators to exploit new attractive services by taking advantage from these cost reductions. 3GPP has formulated the Non-Terrestrial Networks (NTNs) [9] specifications in Release 15 [10] encompassing LEO satellite constellations for the access segment. Such networks present themselves with lower costs than in the early 2000s, and thus appear as a reasonable choice to provide worldwide continuous coverage for ubiquitous connectivity.

The associate editor coordinating the review of this manuscript and approving it for publication was Vittorio Camarchia.

For IoT, providing connectivity to remote endpoints for data collection and aggregation of aerial/maritime traffic for tracking and data services will become a major component in future networks. Another relevant scenario is the case of interconnecting isolated Wireless Sensor Networks (WSNs) located at unreachable places by terrestrial networks, such as polar regions, deserts, seas, tropical rainforests, etc. Transmitters at ships, vessels, planes, or WSN Ground Station (GS) gateways, regularly send critical telemetry messages for position updates or whole aircraft/vessel/sensor trunking data (e.g. web browsing or periodic reports) through the constellation network. Such messages are for tracking of containers in logistics, data from ships/vessels using VHF Data Exchange System (VDES) [11], former Authentication Identification System (AIS) [12], or the Automatic Dependent Surveillance-Broadcast (ADS-B) system [13] in airplanes. In all these scenarios, application end users are interested in reduced delays when compared with other services, to ensure timely updates for a real status monitoring or acceptable Quality of Service (QoS).

Besides propagation and transmission delays, queuing delays pose their own inherent challenges, since these depend not only on transmission and processing capabilities of the satellites, but also on the incoming traffic of the aggregated services. The classical queuing theory from Jackson networks [14], [15] and, in particular Burke and Jackson's Theorems [16], [17], allows us to model such delays over the end-to-end LEO network. However, most approaches assume ideal communication channels as either constant or with fixed statistics and no additional delays. Although the communication channels across the constellation Inter-Satellite Links (ISLs) might be time invariant, satellite-to-ground and ground-to-satellite channels typically display time-varying statistics due to multi-path interference from environment scatters. This results in different channel coefficient means and variances across periods of time, as in the LMS channel proposed in [18]. This behavior directly impacts on the queuing delay, since different channel states might completely block the received signal, thus leading to perceived inactivity periods in the satellite transmitter queues due to intermittent disconnections. Moreover, the possibility that different communication paths can be formed across the constellation, introduces background traffic in the satellites, which might impact even more the performance of an established path. Therefore, accurate analysis of the queuing delay in these scenarios requires to incorporate such aspects. Although there have been works studying queuing models for LEO constellations, most of them focus on either ideal channels or those with single fixed statistics, since their purpose has been to focus on initial estimates.

Opposed to that, we consider a new model for the queuing delay of LEO satellite constellations, where traffic is aggregated from a remote ground station and conveyed to a destination ground station for network monitoring and data analysis. While conventional models assume ideal or fixed channel statistics, we incorporate the aspects of real time-varying channel measurements of the LMS on suitable frequency bands for typical IoT services. We present a theoretical framework, and validate it comparing its results with those yielded by a system-level simulator. Furthermore, the simulator can be also used under other similar scenarios or technologies, where the theoretical assumptions do not hold. Our contributions are the following:

- We introduce a theoretical model based on Quasi-Birth-Death (QBD) processes for evaluating the queuing delay of LMS links, for different states in the satellite-to-ground/ground-to-satellite links, through a generalized Markov chain capturing the different channel states.
- We broaden our model to consider LEO constellation communication paths, to assess their end-to-end delay, based on Open Jackson Networks theory, where inter-satellite links are modeled as lossless $M/M/1$ queues.
- We validate our model, comparing it with system-level simulations that consider empirical channel statistics obtained from real measurements of the LMS channel.
- We compute the end-to-end delay distribution for an established communication path, and we study the effect of the background traffic in the overall delay.
- We exploit the simulator to assess the performance under different assumptions of traffic pattern and packet length distributions.

Our work is structured as follows: Section II discusses prior related work of queuing models for the delay in LEO satellite networks. Section III presents our model for LEO constellations that interconnect ground stations on Earth carrying different traffics flows. In Section IV, we introduce our queuing model based on QBD processes and we also discuss its integration with the LMS channel model. Our results on the queuing delay, which also considers propagation and transmission delays, are discussed in Section V. Final conclusions are drawn in Section VI.

II. STATE OF THE ART REVIEW

The study of queuing delay in LEO satellite networks has been previously considered for different purposes. The authors in [19] proposed a Markov chain to study the storage queue of a single satellite with downlink/uplink on-board capability and a selective-repeat Automatic Repeat Request (ARQ) process for error correction. They consider packet erasures in the transmission links and propose the queuing model for finding optimal storage buffers. The work in [20] reviews the end-to-end delay of LEO satellite constellations with a simulation framework using capacity and flow optimization, but their estimates of the queues are not reported. Authors in [21] propose a delay model that considers not only the queuing but also the propagation delay for a Galileo-like satellite constellation. The authors model the delay in the ISLs both for intra- and inter-planes, with two different routing policies. In this case, they consider that the delay can be modeled as a Markov chain with eight states. However, their

results appear hard to generalize, since they depend on a fixed topology with very specific delay distributions.

Another study for the queuing delay in optical LEO constellations is found in [22], where the authors calculate the average number of ISLs between two GSs to compute an average queuing delay, considering Poisson-distributed incoming traffic, but without evaluating potential queuing situations. A study for a queuing model in Software-defined Networking (SDN) satellite networks is proposed in [23]. This work models the queuing delay in Delay-Tolerant Networks (DTNs), which considers the signaling process and store-and-forward mechanism of satellite nodes, given plausible disconnection times. However, it does not take into account the impact of satellite channel time-varying aspects, by assuming an ideal setup, which is not realistic in practical scenarios. It focuses on the effect of the SDN controller in Geostationary Orbit (GEO) orbit, excluding non-SDN scenarios. Similarly, the performance of SDN-based Routing Algorithm (SDRA) is quantified, in terms of queuing delay and total hop distance for LEO constellations, in [24], where the controllers are interconnected through the GSs in a terrestrial network. Still, their adopted queuing model considers ideal constant channels while trying to avoid overloading satellite queues.

More recently, an analysis of intermittent satellite links in LEO and Medium Earth Orbit (MEO) constellations is discussed in [25]. The authors propose a two-state Markov to model working and vacation periods. These periods are a function of the Line of Sight (LoS) times between two satellites, or a satellite and a ground station, and not strictly of the queue length. Even though being a useful approach, it does not provide a realistic channel model since it focuses only in the constant channel case under the visibility period. The work in [26] considers system simulations of traffic to estimate the ideal buffer size for avoiding bufferbloat, when considering queuing delay in GEO or MEO links, and its impact over Transmission Control Protocol (TCP) performance. The study considers the adaptation of real world traffic flow distributions, which are integrated as traces into the simulation environment, and these are then used to analyze the traffic queues and obtain optimum buffer sizes. Still, it does not capture the general case of time-varying channels, particularly for the satellite-to-ground links, since it focuses on the packet loss effect in the TCP data transfer period, rather than the underlying causes of the loss.

Authors in [27] design a Queue State-based Dynamic Routing (QSDR) for LEO, where the queue state is only estimated from the available number of packets in the satellite queue. The average and instantaneous queue lengths are weighted and combined to provide a reasonable estimate, which needs to be tailored for specific scenarios. Different queuing models for LEO constellations are introduced in [28] to analyze the communication path survivability, i.e., the probability of successful operation without attacks in the chosen path, based on a utility function that considers the communication costs. These models consider the reception buffers for a constrained number of accessing nodes, satellite processing and transmission to the next node. However, the authors still envision ideal channel conditions for both up- and downlink. A more recent queuing model for a similar constellation that the one we consider herewith is discussed in [29], where the authors analyze the Age of Information (AoI) as a function of the queuing delay. The considered scenario comprises various satellites connecting a set of devices towards a destination GS, whose traffic gets aggregated by an initial satellite in the path. The intermediate satellites may add further incoming traffic on their own, as well as background traffic, loading the next satellites in the path. In [30] and [31], the same authors propose the use cases of either offloading a local 5G cellular network, and backhauling where nearby mobile networks are not present. The authors consider, in these last three works, $M/M/1$ queues for any satellite communication path, assuming that communication channels do not vary along time.

Opposed to existing works, we propose a novel model to characterize the end-to-end delay in LEO constellations. We consider the variability that LMS channels might have, by proposing a novel Markov-chain model that captures the time-varying characteristics of these links. Then, we use queuing theory to assess the average end-to-end-delay through an established path in a path of a LEO constellation with ISLs with ideal channels in space. Furthermore, by exploiting a proprietary event-driven simulator, we also study the variability of such delay, which might strongly affect the behavior of services having real time requirements (for instance IoT based services, such as telemetry). To the authors' best knowledge, and considering the aforementioned existing state-of-the-art, this is the first work that tackles this analysis.

III. LEO SATELLITE CONSTELLATION MODEL

We consider a generic LEO "Streets of Coverage" satellite polar constellation [32] for full Earth coverage, which consists of N satellites arranged in P orbital planes at a given orbit height h, and with S satellites per plane. Satellites that are at the same orbital plane possess the same orbital parameters. We thus consider circular orbital planes (i.e. null eccentricity) rotating separated by $180°/P$ from each other. In each plane, satellites are separated by an angle of $360°/S$. We consider two generic GSs located at two different points of Earth, and connected through a communication path across one of such planes formed by an Up Link (UL), set of ISLs and Down Link (DL) across the constellation network, shown in Figure 1 for the example case of three satellites. The satellites interconnect a WSN with a Network Control Center (NCC), for which we define a traffic flow of rate λ described in Section III-B. For our queuing delay estimates, we consider this network as a *static snapshot*, since the queuing delay time horizon is much more smaller than the time horizon for topology changes. Typical times for a defined communication path at LEO heights are in the order of 10-20 minutes [32].

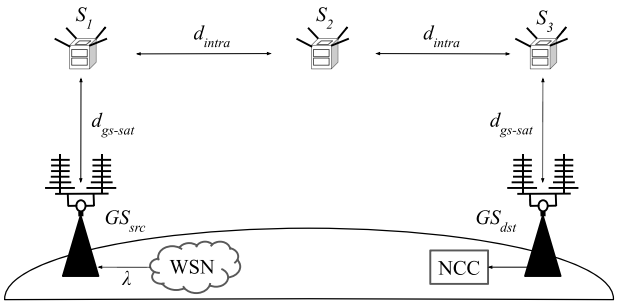

FIGURE 1. A path of three satellites in the same orbital plane connecting two ground stations. The WSN generates traffic with rate λ through the satellites and towards the NCC.

In this way, our model does not exclude different orbital planes for the ground stations.

A. MINIMUM NUMBER OF SATELLITES & DISTANCES

The minimum number of satellites for global coverage with LEO constellation for a given orbit height h and minimum elevation angle ε_{min} are calculated as described in [33]. Such constellation design ensures all satellites have LoS with their nearest neighbors. We can straightforwardly compute the Earth half-center angle θ_{GS}, shown in Figure 2. The coverage of any given satellite for a given orbit height h and minimum elevation above horizon ε_{min} is defined as follows [32]:

$$\theta_{GS} = \frac{\pi}{2} - \arcsin\left(\frac{R_E \cos(\varepsilon_{min})}{R_E + h}\right) - \varepsilon_{min} \tag{1}$$

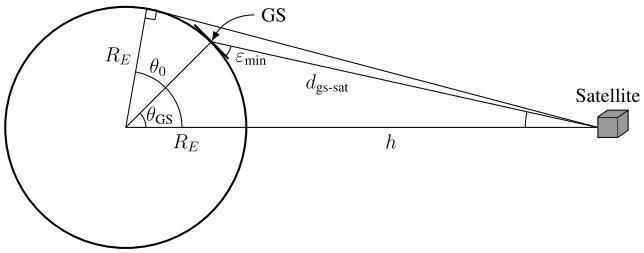

FIGURE 2. Coverage design geometry.

where R_E is the radius of the Earth. Then, the total number of satellites for a given λ_{GS} is [33]:

$$N = \frac{4}{1 - \cos(\theta_{GS})} \tag{2}$$

From Figure 2, the GS-to-satellite distance is defined as:

$$d_{gs-sat} = \sqrt{2R_E h + h^2 + (R_E \cos(\varepsilon))^2} - R_E \cos(\varepsilon) \tag{3}$$

Similarly, from the constellation geometry, the intra-satellite distance between neighboring satellites in the same plane is:

$$d_{intra} = (R_E + h)\sqrt{2\,(1 - \cos(2\pi/S))} \tag{4}$$

B. TRAFFIC FLOW MODEL

Under the path between the two ground stations GS_{src}, GS_{dst} in Figure 1, the source GSs aggregates traffic from a WSN and forwards it to another remote destination GS connected to the NCC for data monitoring and analysis. The closest satellite to the originating GS conveys such traffic to other satellite constellations from the UL during its pass when in visibility and having a local elevation angle $\varepsilon \geq \varepsilon_{min}$ from the local horizon. Similarly, the terminating GS offloads its carrying traffic at the DL.

A *poissonian* traffic pattern with rate parameter λ is considered for the total aggregated traffic flow from the WSN at GS_{src}, which originates from aggregating periodic messages of telemetry reporting from an arbitrarily large number of identical IoT devices. This assumption is reasonable, as discussed in [34]. The traffic is generated from GS_{src} to GS_{dst} across K satellites in a constellation plane in general.

The fixed distance between the satellites defines the propagation delay as $\zeta = d_{\text{intra}}/c$ (or d_{gs-sat}/c for UL/DL) where c is the speed of light in vacuum. The satellites transmit equal priority of exponentially-distributed application packets of average length ℓ, with previously allocated resources and a transmission capacity $\mathcal{C}$, given by the effective transmitter interface bit rate. We consider that there are not errors in the links, or if so, capacity data rates are reduced to have effective link budgets within constrained satellite power and arbitrarily small errors, so no packet losses nor retransmissions are introduced in the communication path.

C. SATELLITE CHANNEL MODELS

We distinguish between two types of links: (i) UL (ground-to-satellite)/DL (satellite-to-ground) links and (ii) ISLs. For intra-ISLs in a plane, we model these as ideal LoS stable links in outer free space, having a constant stable connection between any two satellite nodes. We thus consider these have a constant service rate (capacity), representative of their communication frequency band. For both the UL and DL channels, we consider the LMS channel defined in [18]. Such channel can be characterized as a three-state Markov Chain, defined by particular conditions. The states are: LoS (exhibiting ideal characteristics), moderate (mid) shadowing (where the service rate is lower than the one that can be achieved for LoS conditions), or deep shadowing (with a service rate that might be considerably much lower than the one that would be seen over ideal conditions). The discrete Markov chain that characterizes the LMS channel is shown in Figure 3, where the transitions between the corresponding states are modeled by means of the corresponding probabilities, i.e. p_{lm} corresponds to the probability of going from the LoS state to the *Mid-Shadowing* state and so on. In Section IV, we discuss how we exploit and extend the LMS channel model to also consider QoS parameters (i.e. delay).

IV. SATELLITE QUEUING ANALYSIS

Our goal is to study the total delay by considering the propagation, transmission, and queuing delay from Jackson

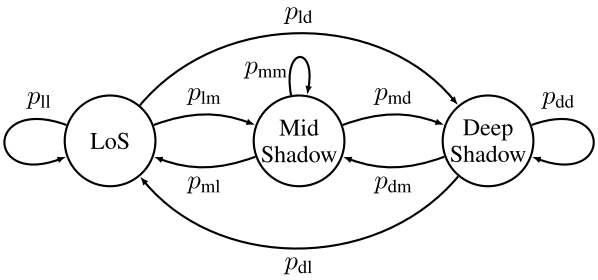

FIGURE 3. Markov chain model for the UL/DL satellite channels.

networks theory. As stated earlier, we consider two types of links: (i) UL/DL, and (ii) ISL. For the latter, we use a $M/M/1$ queue with arrival rate $\lambda_k = \lambda$, service rate μ_k, being $\rho_k = \lambda_k/\mu_k$ the traffic utilization factor $\forall k = 1, \ldots, K-1$. The underlying assumption is that ISLs show a rather predictable LoS stable behavior, allowing that the transmission capacity does not vary for processing the packets. The number of such $M/M/1$ nodes is $K-1$, since there are $K < S$ satellites connecting the stations. We consider infinite buffers, since under sensible loads, the results we present later show that the probability of long queues is low. Finite buffer analysis is left for our future work. We also consider that served packets follow a First-Come First-Serve (FCFS) policy for all satellites, given that packets are processed as soon as possible. Table 1 summarizes all the variables in our model.

A. UPLINK/DOWNLINK QUEUING MODEL

For the UL and DL ($k = 0, K$ respectively), we consider the bi-dimensional Markov Chain shown in Figure 4, where packets arrive following a Poisson process with arrival rate λ. As we mentioned previously, we consider the channel features between ground station and satellite (or vice versa) that can be captured with the LMS model. We thus assume three different service rates in the k^{th} link, each of them corresponding to each of the channel states: μ_{los}, μ_{ms}, μ_{ds}, for LoS, *Mid-Shadowing*, and *Deep-Shadowing*, respectively. Such service rates can be established based on the effective capacity of the link under each of the three states: $\mu_s = \frac{\ell}{\mathcal{C}_s}$, where ℓ is the average packet length, and $\mathcal{C}_s$ is the effective capacity for each of the states, $s = \{\text{los, ms, ds}\}$.

As can be seen in Figure 4, each channel condition is represented by a row in the Markov chain, while states are represented by a tuple (i, j), where i reflects the number of packets at the link (either being transmitted or waiting at the buffer in the outgoing interface), and j the current channel status: LoS (2), *Mid-Shadowing* (1), or *Deep-Shadowing* (0). In each row, packet arrival is captured by a rightwards transition (rate λ), while a leftwards transition mimics a packet being successfully transmitted to the next hop.

The time that the channel stays at a particular situation is modeled by means of an exponential random variable, with mean $\eta_{\text{los}}^{-1}, \eta_{\text{ms}}^{-1}, \eta_{\text{ds}}^{-1}$. The queuing model we propose is based on a continuous Markov chain, and we thus need to use the transition probabilities from the original LMS model

TABLE 1. Model variables.

λ	Packet arrival rate
ℓ	Average packet length
μ_s	Service rate of the s LMS state $s = \{\text{los, ms, ds}\}$
p_{sr}	Transition probability between LMS states s and r $s, r = \{\text{l (los), m (ms), d (ds)}\}$
δ	Time slot (channel state transitions)
η_s	Inverse of sojourn time at state s $s = \{\text{los, ms, ds}\}$
α_{sr}	Probability of going to state r after leaving s $s = \{\text{l (los), m (ms), d (ds)}\}$ and $s \neq r$
ξ_{sr}	Transtion rate between channel states s and r $\xi_{sr} = \eta_s \cdot \alpha_{sr},\ s = \{\text{l (los), m (ms), d (ds)}\}$ and $s \neq r$
μ_{mm1}	Service rate of the $M/M/1$ links, $\mu_{\text{mm1}} = \mu_{\text{los}}$
ρ_{mm1}	Occupancy of the $M/M/1$ links, $\rho_{\text{mm1}} = \frac{\lambda}{\mu_{\text{mm1}}}$
K	Number of satellites
ζ_k	Propagation delay of the k$^{\text{th}}$ link, $k = 0, \ldots, K$
$\pi_i(j)$	Probability of state (i,j) There are i packets and LMS is in state j $j = \{2\ \text{(los)}, 1\ \text{(ms)},\ 0\ \text{(ds)}\}^\intercal$
π_i	Column vector: $[\pi_i(0)\ \pi_i(1)\ \pi_i(2)]$
$\mathcal{Q}$	Infinitesimal matrix of the QBD process
F	Forward transition matrix
B	Backward transition matrix
L, L_0	State transition matrices within the same level
$\overline{N_{\text{lms}}}$	Average number pf packets at the UL/DL links
$\overline{N_{\text{mm1}}}$	Average number of packets at the ISL
τ_{lms}	Delay at the UL/DL links
τ_{mm1}	Delay at the ISL
$\mathcal{R}$	Routing matrix
γ_k	Background traffic rate on the k^{th} link
Λ	Row vector with traffic rate at each node
Γ	Row vector with external traffic arriving at each node

(see Figure 3) to establish such times. The discrete chain that was introduced in [18] assumes that a transition might happen at every time slot, and we thus need to consider its duration to convert it to a continuous random variable. The following establishes the mean value of such time.

Lemma 1: The average time that the UL/DL channel stays at a particular condition (according to the LMS model introduced in [18]) can be calculated as:

$$\eta_s^{-1} = \frac{\delta}{1 - p_{ss}} \tag{5}$$

where s = los/l, mid-shadowing/m, deep-shadowing/d, δ is the corresponding slot time, when channel transitions might happen, and p_{ss} is the probability of staying at the same state s.

Proof: The number of consecutive time slots that the LMS channel states at the same status follows a geometric random variable, with mean $(1 - p_{ss})^{-1}$. The average state duration is obtained multiplying such mean value by the duration of each time slot, δ. □

In the proposed model, whenever the corresponding link leaves one condition (s), it can go to one of the other remaining ones (r, t). The corresponding probabilities can be calculated as follows:

$$\alpha_{sr} = \frac{p_{sr}}{p_{st} + p_{sr}}; \quad \alpha_{st} = \frac{p_{st}}{p_{st} + p_{sr}} \tag{6}$$

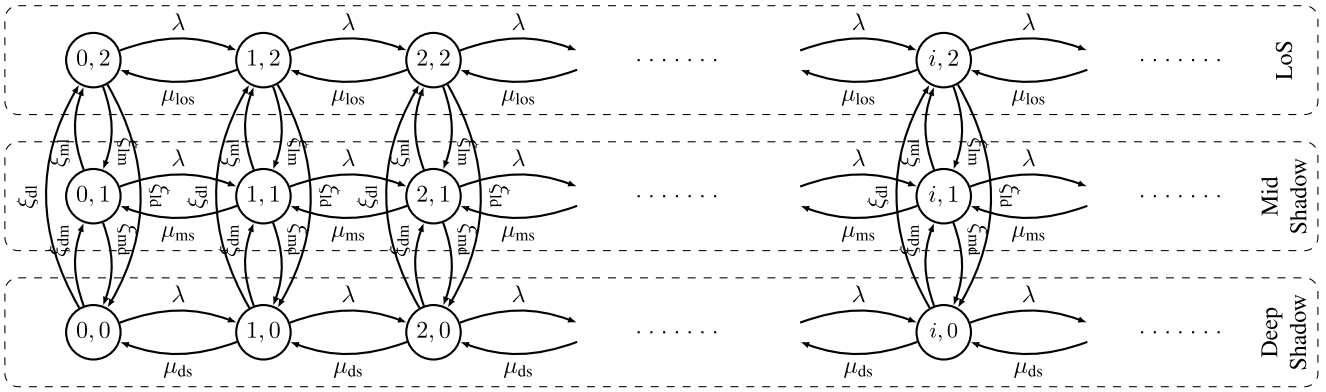

FIGURE 4. Markov Chain model for the LMS links.

where s, r, t = los/l, mid-shadow/m, deep-shadow/d, and $s \neq r \neq t$. This is reflected in Figure 4 by means of the corresponding transition rates: $\xi_{sr} = \alpha_{sr}\eta_s$, which capture the vertical transitions in the proposed Markov chain.

To properly generalize its analysis, we first note that the proposed model corresponds to a QBD process, since it has transition matrices with a block structure, as will be discussed shortly. We will thus use the Matrix Geometric Method, thoroughly discussed in the seminal works of Neuts [35] and Hajek [36], to obtain the behavior of the LMS link. We first define $\mathcal{Q}$ as the infinitesimal generator matrix of the corresponding QBD process:

$$\mathcal{Q} = \begin{bmatrix} L_0 & F & 0 & 0 & \cdots \\ B & L & F & 0 & \cdots \\ 0 & B & L & F & \cdots \\ \vdots & & \ddots & & \ddots \end{bmatrix} \tag{7}$$

where each element corresponds to a 3×3 matrix, which are given in (8), as shown at the bottom of the next page. We define the stationary distribution of the system as: $\Pi = [\pi_0, \pi_1, \ldots]$, where each π_i is a column vector of length 3, so that $\pi_i(j)$ is the probability of having i packets in the node, when the link is in status j: LoS (2), *Mid-Shadowing* (1), or *Deep-Shadowing* (0).

Assuming the system has a stationary solution (i.e. it works in a stable operation regime), there exists a constant matrix R so that [37, Theorem 3.1.1]:

$$R^2B + RL + F = 0 \tag{9}$$

where all $R,\ B,\ L,\ F \in \mathbb{R}^{3\times3}$. In addition, there is a unique positive solution to the finite system of equations [37]:

$$\pi_0^\intercal\,(L_0 + RB) = \mathbf{0}^\intercal; \quad \pi_0^\intercal\,(I-R)^{-1}\,\mathbf{1} = 1 \tag{10}$$

where I is the 3×3 identity matrix, and $\mathbf{0}, \mathbf{1}$ are all-zeros and all-ones column vectors of length 3, respectively. Then, $\Pi = [\pi_0, \pi_1, \ldots]$ is given by:

$$\pi_i^\intercal = \pi_0^\intercal R^i \tag{11}$$

Since there is no straightforward closed solution for the quadratic equation in (9), an iterative method can be used to find R. With the stationary distribution, we obtain the average number of packets and per packet delay with Little's Law as:

$$\overline{N_{\text{lms}}} = \left\| \frac{\pi_1}{(I-R)^2} \right\|_1 = \left\| \frac{\pi_0^\intercal R}{(I-R)^2} \right\|_1; \quad \tau_{\text{lms}} = \frac{\overline{N_{\text{lms}}}}{\lambda} \tag{12}$$

where the delay includes both the waiting and transmission times. The stationary distribution is only guaranteed if the average service rate of the link is higher than the incoming data rate, and we can thus establish the maximum packet rate that ensures system stability and so the model validity as:

$$\lambda_{\max} = \sum_{j=0}^{2} \theta_j \mu_j \tag{13}$$

where θ_j is the probability that the LMS stays at a particular condition, which can be found by solving:

$$\Theta^\intercal A = \mathbf{0}^\intercal; \quad \Theta^\intercal \mathbf{1} = 1 \tag{14}$$

where Θ is a column vector of length 3, with the probability of each of the LMS states: $\Theta = [\theta_0, \theta_1, \theta_2]^\intercal, A = L + B + F$.

B. END-TO-END DELAY

We consider the system queuing diagram in Figure 5. It shows the path between the two terrestrial stations connected through a chain of K satellites with their queues, $S_1, S_2, \ldots S_K$. As can be seen, both the first (UL, from GS_{src} to S_1) and last (DL, from S_K to GS_{dst}) links are modeled with the Markov chain that we have previously introduced. The remaining links (from S_k to S_{k+1}, $k = 1, \ldots K-1$) are modeled with the traditional $M/M/1$ queuing system.

We can use Open Jackson Networks theory [14], [15] and, in particular Burke and Jackson's Theorems [16], [17], to establish the performance of such topology. If there is no other traffic flow, we can sum the average number of packets at each link, and then establish the overall delay as:

$$\tau_{\text{total}} = \frac{\overline{N_{\text{lms}}} + \sum_{k=1}^{K-1} \left(\overline{N_{\text{mm1}}}\right)_k + \overline{N_{\text{lms}}}}{\lambda} + \sum_{k=0}^{K} \zeta_k \tag{15}$$

$$= \tau_{\text{lms}} + \sum_{k=1}^{K-1} (\tau_{\text{mm1}})_k + \tau_{\text{lms}} + \sum_{k=0}^{K} \zeta_k \tag{16}$$

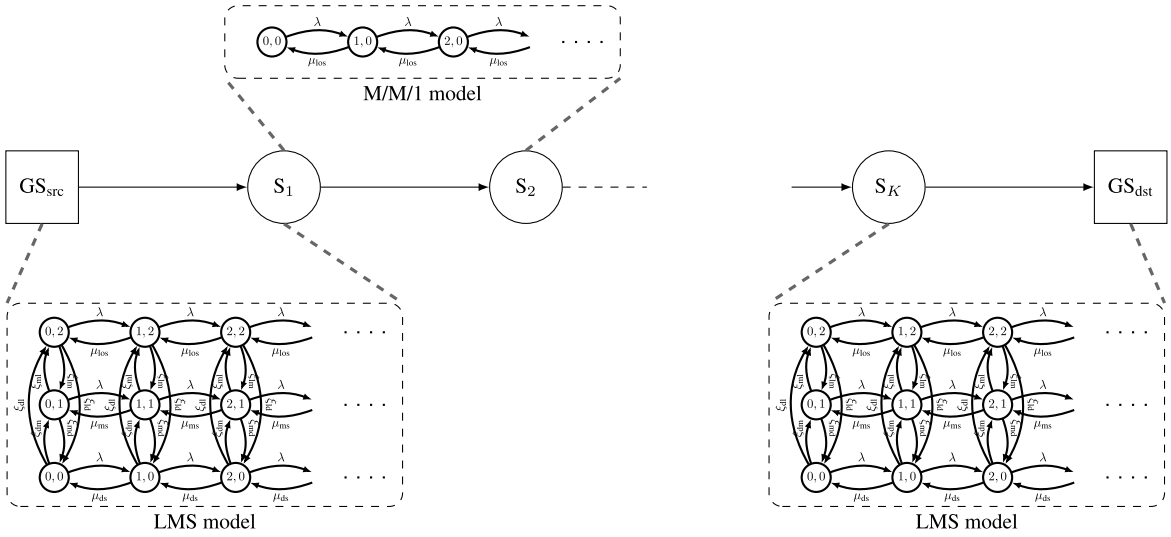

FIGURE 5. Markov Chain model for the satellite nodes.

where $\overline{N_{\text{lms}}}$, τ_{lms} are the average number of packets, and the delay for the LMS links, respectively, given by (12); $\left(\overline{N_{\text{mm1}}}\right)_k$, $(\tau_{\text{mm1}})_k$ are the corresponding values for the k^{th} $M/M/1$ ISL link, given by (17), and ζ_k is the propagation delay of the k^{th} link.

$$\left(\overline{N_{\text{mm1}}}\right)_k = \frac{\rho_{\text{mm1}}}{1-\rho_{\text{mm1}}} \quad , \quad (\tau_{\text{mm1}})_k = \frac{1}{\mu_{\text{los}}-\lambda} \tag{17}$$

Equation (16) is valid only if the conditions of the Burke and Jackson's Theorems hold. In this sense, the output process of the first LMS link should correspond with a Poisson process of rate λ. This can only be guaranteed if $\mu_{\text{ds}} > \lambda$, i.e. the slower service rate (which corresponds to the *Deep-Shadowing* channel condition) is higher than the incoming packet rate. If this is not the case, even if the model is stationary and so works in a stable regime, the real overall delay would be higher, as will be seen later.

C. BACKGROUND TRAFFIC

The proposed model can also be used to consider background traffic, when some of the links are used by other flows. In this case, we can calculate the overall incoming packet rate at the k^{th} link as: $\lambda_k = \lambda + \gamma_k$, where γ_k is the overall background traffic for such link. For analyzing more complex network deployments, with several nodes having background traffic, and more end-to-end communication, we could establish the routing matrix, $\mathcal{R}$, where $r_{n,m}$ is the probability for a packet exiting link n to go to link m. In the case of a single end-to-end chain (as the one that will be analyzed in Section V), with some nodes having background traffic, it is straightforward to see that $r_{n,n+1} = \frac{\lambda}{\lambda+\gamma_n}$ and zero otherwise. Hence, we could obtain the incoming packet rate at every node as follows:

$$\Lambda = \Gamma\,(I-\mathcal{R})^{-1} \tag{18}$$

where Λ is a row vector, with the overall packet rate at each node, and Γ is another row vector with the external traffic, including the background traffic at each node.

V. RESULTS & DISCUSSION

In this section, we first assess the validity of the proposed queuing model by exploiting an event-driven simulator[1] implemented in C++. We compare the results from the Jackson Networks theoretical framework with those obtained from the simulator. Later, the simulator permits to broaden the analysis in situations where the conditions required to apply the theoretical framework do not hold, i.e. when the packet arrival rate is higher than the service rate of the LMS links, when these stay at the *Deep-Shadowing* condition.

The simulator considers two types of links: LMS and ISL (i.e. the $M/M/1$ queue). Whenever a packet exits a node,

[1] https://github.com/tlmat-unican/queuing-leo

$$F = \begin{bmatrix} \lambda & 0 & 0 \\ 0 & \lambda & 0 \\ 0 & 0 & \lambda \end{bmatrix} \quad B = \begin{bmatrix} \mu_{\text{los}} & 0 & 0 \\ 0 & \mu_{\text{ms}} & 0 \\ 0 & 0 & \mu_{\text{ds}} \end{bmatrix} \quad L_0 = \begin{bmatrix} -(\lambda+\eta_{\text{los}}) & \xi_{\text{lm}} & \xi_{\text{ld}} \\ \xi_{\text{ml}} & -(\lambda+\eta_{\text{ms}}) & \xi_{\text{md}} \\ \xi_{\text{dl}} & \xi_{\text{dm}} & -(\lambda+\eta_{\text{ds}}) \end{bmatrix}$$

$$L = \begin{bmatrix} -(\lambda+\mu_{\text{los}}+\eta_{\text{los}}) & \xi_{\text{lm}} & \xi_{\text{ld}} \\ \xi_{\text{ml}} & -(\lambda+\mu_{\text{ms}}+\eta_{\text{ms}}) & \xi_{\text{md}} \\ \xi_{\text{dl}} & \xi_{\text{dm}} & -(\lambda+\mu_{\text{ds}}+\eta_{\text{ds}}) \end{bmatrix} \tag{8}$$

or there is a new packet arrival, the simulator decides which node should process it. Then it checks the status at such node: if the interface is empty, the packet will begin with its transmission, and the corresponding end-of-transmission event will be scheduled; otherwise, the packet will be kept at the buffer until it can be eventually transmitted. Therefore, there are two types of packet-related events: (1) arrival of a new external packet; (2) end of a packet transmission. On the other hand, for the UL/DL LMS channels, the simulator handles another event that, upon expiration, changes the corresponding channel condition. It uses the corresponding probabilities introduced in Figure 3 to establish the next channel status, and based on its average duration, correspondingly schedules the next change. We can include as many external flows as desired. We will first stick to Poisson arrival processes (i.e. packet inter-arrival times are exponentially distributed) and exponential transmission times, to assess the validity of the proposed model, but we will also configure the simulator to consider different distributions for these two parameters.

TABLE 2. Model variables, assuming S band and a suburban area, LMS parameters are obtained from [18, Table 3].

LoS Capacity, R_b	5 `Mbps`
Mid-Shadow Capacity	$0.1R_b$
Deep-Shadow Capacity	$0.01R_b$
Average packet lengths, ℓ	$\{100, 1000\}$ `Bytes`
# of satellites in the path, K	6
Constellation height	1000 km
ISL distances	7378 km
LMS transition probabilities 0 (los), 1 (ms), 2 (ds)	$P_{40^o} = \begin{pmatrix} 0.8177 & 0.1715 & 0.0108 \\ 0.1544 & 0.7997 & 0.0459 \\ 0.1400 & 0.1433 & 0.7167 \end{pmatrix}$
	$P_{60^o} = \begin{pmatrix} 0.8019 & 0.1314 & 0.0667 \\ 0.1386 & 0.7596 & 0.1018 \\ 0.1242 & 0.1032 & 0.7726 \end{pmatrix}$
	$P_{80^o} = \begin{pmatrix} 0.8177 & 0.1715 & 0.0108 \\ 0.1544 & 0.7997 & 0.0459 \\ 0.1400 & 0.1433 & 0.7167 \end{pmatrix}$
LMS states probability 0 (los), 1 (ms), 2 (ds)	$\mathcal{P}_{40^o} = [0.4545\ 0.4545\ 0.0910]$
	$\mathcal{P}_{60^o} = [0.4000\ 0.3333\ 0.2667]$
	$\mathcal{P}_{80^o} = [0.1428\ 0.4286\ 0.4286]$
Slot time, δ	100 μs

A. LMS QUEUING MODEL VALIDATION

We first focus on the validation of the QBD process that we have used to mimic the behavior of the LMS channels. We consider the parameters that are depicted in Table 2. In our simulations, we consider the S frequency band at 2.6 GHz as representative of IoT telemetry aggregation, and that the capacity of the link under LoS ideal conditions is 5 `Mbps`. We also assume that the service rates at the *Mid-Shadowing* and *Deep-Shadowing* conditions are 0.1 and 0.01 times the ideal one, respectively, since we compensate deep fading in the link budgets (10 dB for mild and 20 dB for deep shadowing) by reducing the rates in the same proportion so that to keep the budget with the same margins approximately. We consider average packet lengths of 100 and 1000 `Bytes` since these are representative of aggregate IoT application traffic [34], [38].

The configuration of the LMS channel model corresponds to a suburban area (from [18]), having generic mild propagation conditions, and we study different elevation angles ε, each of them with different transition probabilities. We use Lemma 1 to establish the corresponding average times at each of the link states, and (6) to calculate the consequent probabilities of going to the next channel status α_{sr}, α_{st}.

Before discussing the obtained results, Table 3 shows that the simulator is able to appropriately capture the dynamics of the LMS channel, as reported in [18]. For each of the parameters, we include the value that was empirically observed using the developed simulator (left column), as well as the theoretical values, which are directly obtained from [18, Table 3]. The state probability captures the fraction of time the link would stay at a particular channel condition in milliseconds. Besides, the state average time corresponds to the sojourn time for each of the three states, where the theoretical values are established with Lemma 1. Last, the transition probabilities correspond to the percentage of times a particular channel state was visited when starting from the one at the corresponding row. In this case, the theoretical values were obtained with (6). As can be seen, the differences between theoretical and simulation-based values are, for all the considered parameters, rather small, so validating the simulator operation range.

1) UL/DL PACKET QUEUES

We compare the probability of having n packets in the UL/DL transmitter, either transmitting or waiting. Figure 6 represents such probabilities, for two values of λ, and assuming an average packet length of 1000 `Bytes`, and an elevation of $\varepsilon = 80°$. For each x-axis value, we plot two stacked bars. The left one (in solid colors) are the values that are theoretically obtained, with the model depicted in Section IV, while the right shaded bars were the outcome of the simulator. For each n value we distinguish the corresponding channel status, with a different color. As can be seen, there is a very accurate match between the theoretical probabilities and the values produced by the simulator. We can observe, in this particular channel configuration, that the probability of being in the LoS situation is only noticeable when the link is idle. Besides, when λ is higher, the occupancy of the link increases, and so the probability of having zero packets in the node is lower.

2) LMS TOTAL DELAY DISTRIBUTION

We then analyze first how the average total delay (sojourn time) and queue waiting time (excluding service) vary against the incoming packet rate. Figure 7 shows both times when λ increases, within the stable regime operation, i.e. $\lambda < \lambda_{\max}$ cf. (13). Lines represent theoretical values, while markers correspond to the simulation results. As can be seen, there is an almost perfect match between them, which validates both the proposed queuing model for the LMS link, as well as the operation of the simulator. We can see that the transfer time remains quite stable (mostly service) until $\lambda \approx \mu_{\text{ds}}$, which

TABLE 3. States probabilities, for each parameter simulated (left) and theoretical (right) values are showed. Theoretical values are obtained at $\varepsilon = 80°$ from [18, Table 3].

	State Prob.		State Avg. Time (*ms*)		Transition Probability					
					LoS		Mid-Shadowing		Deep-Shadowing	
LoS	0.1393	0.1428	341.036	366.032	n.a.		0.6137	0.6070	0.3863	0.3930
mid-Shadowing	0.4268	0.4286	504.027	500.25	0.2637	0.2676	n.a.		0.7363	0.7304
deep-Shadowing	0.4338	0.4286	558.596	547.046	0.2206	0.2139	0.7794	0.7861	n.a.	

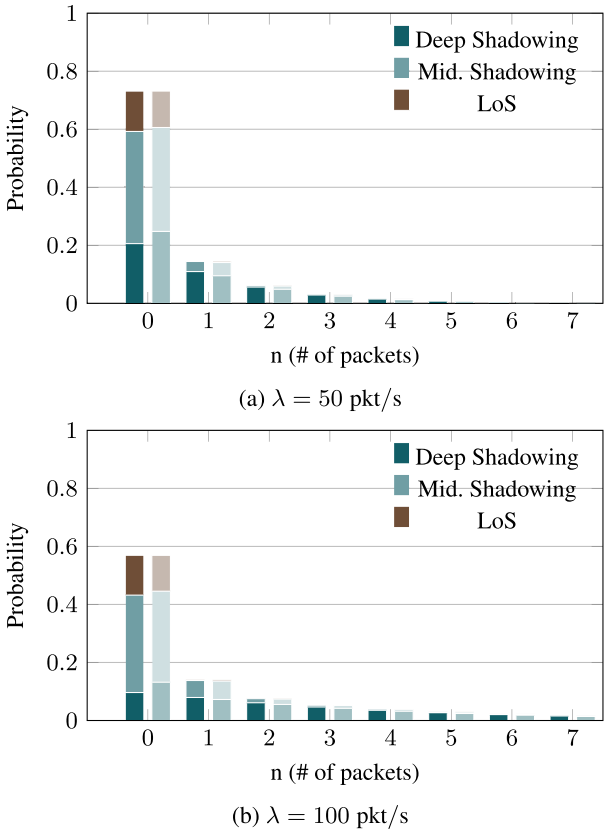

FIGURE 6. Probability of having n packets in the node for $\varepsilon = 80°$ and $\ell = 1000$ `Bytes`. Model and simulation results are shown with solid and shaded colors respectively.

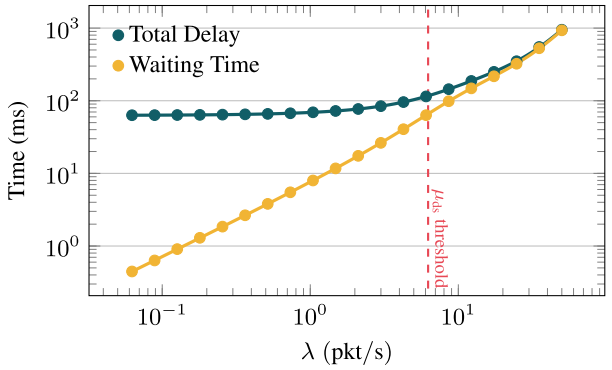

FIGURE 7. Comparison of simulated and theoretical results of node delay and waiting time for different λ values $\ell = 1000$ `Bytes`. Theoretical and simulated values are shown with solid line and markers, respectively.

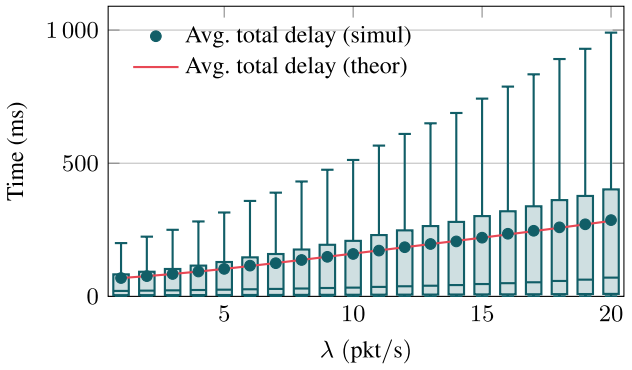

FIGURE 8. Box-and-whisker plot of the total delay distribution for an elevation $\varepsilon = 80°$ and average packet length of $\ell = 1000$ `Bytes`. The results are obtained from a single simulation where 10^6 packets are transmitted. Theoretical and simulated average values are shown with a red solid line and green markers, respectively.

has been reflected by a vertical dashed line and where we used logarithmic representation for the sake of clarity. After such value, the total sojourn time increases at a quicker pace, and this might hinder reaching delay requirements.

Besides assessing the validity of the proposed model, the simulator can also be exploited to broaden the analysis. In this sense, we can use it to study not only the average sojourn delay in the LMS link, but also its variability, which is a relevant metric for services with highly reliable estimates, especially those with stringent real-time requirements. We carry out a number of experiments for various λ values, each of them encompassing the transmission of 10^6 packets. We then use a box-and-whisker plot (boxplot) representation in Figure 8 for the dispersion of the observed total delays. Each boxplot represents: the median (50^{th} percentile), with the horizontal line within the box, the 75^{th} and 25^{th} percentiles (upper and lower box limits, respectively), as well as the 95^{th} and 5^{th} percentiles (upper and lower whiskers, respectively). In addition, we have added, with green markers and a red solid line, the average total delay (for simulation-based and theoretical results, respectively). As can be observed, the traffic increase does not only yield a longer average delay, but the corresponding variability also suffers a sharp increase. In this sense, it is worth noting the great difference between the average delay and the 95^{th} percentile, which is about 100% larger. This reflects a clear long-tailed distribution, and even if the delay of most packets might be reasonable, there exist a large number of them that suffer much greater delays.

B. END-TO-END DELAY

Once the queuing model for both the UL and DL has been validated, we now proceed to study the end-to-end delay between two ground stations, which use a ring of $K = 6$ satellites to establish a communication path. As we mentioned before, this type of scenario is representative and of importance for delay-sensitive applications when dealing with real-time information. We exploit the theoretical model discussed in Section IV, and thus consider that each of the five ISLs are modeled as a $M/M/1$ system, with capacity equal to that in LoS (i.e. 5 `Mbps`). We then compare with event-driven simulator results.

1) END-TO-END AVERAGE TOTAL DELAY

Figure 9 shows the average total delay between the source and destination for two different packet lengths (100 and 1000 `Bytes`). The solid lines correspond to the analytical model, while the markers are the results that were obtained with the simulator, averaging 100 independent experiments, each of the comprising the transmission of 10^4 packets. As can be seen, there is again an almost precise match between the two approaches, validating both the proposed model and the simulator. The incoming rate λ is increased for both packet lengths, from a low value to μ_{ds} since, as was discussed before, the model would not be valid when the outgoing process of the UL is not adhering to Poisson statistics, as it would happen for packet rates greater than the lowest service rate. As can be seen, the elevation of the first/last links has a strong impact over the end-to-end delay due to the reported statistic of the LMS channel. It also increases at a quicker pace (i.e. the slope of the corresponding curves is higher).

2) END-TO-END TOTAL DELAY DISTRIBUTION

Besides the average end-to-end delay, for certain services it also becomes relevant to study its variability (i.e. jitter). As we did earlier for the LMS link, we exploit the simulator to analyze how variable are the observed delays. We carry an experiment setup with longer packetson average (1000 `Bytes`), and do not restrict packet arrival rates to be always lower than μ_{ds}. This is set to observe whether there is a relevant difference between the analytical and the simulator delays, but when the restriction of having a real Poisson process at the output of all nodes is not respected.

Figure 10 shows the variation of the end-to-end delay, using box-and-whisker plots. We can see that when the packet arrival rate gets higher, besides the increase on the average end-to-end delay, the variability might be significant. In this sense, even if the average delay stays below a certain value, there might be packets suffering much longer delays. We can also conclude that the main cause for this high variability are the LMS links, since each of the two links would have the behavior depicted in Figure 8, which corresponds to most of the variability seen for the end-to-end delay. It is important to keep in mind that the intermediate nodes are working a small percentage of their capacity and they do not thus yield much uncertainty. We study later the impact of increasing the occupancy of such links. Also, Figure 10 yields that despite the analytical model is restricted by the lowest service rate (μ_{ds}), the difference between the theoretical and real performances beyond such value (vertical red dashed line) is not substantial, although the y-axis scale is rather wide. For the highest λ value (more than 3 times μ_{ds}), the end-to-end delay yielded by the analytical model is ≈ 55 ms smaller than the value obtained with the simulator, yielding a difference of $\approx 8\%$.

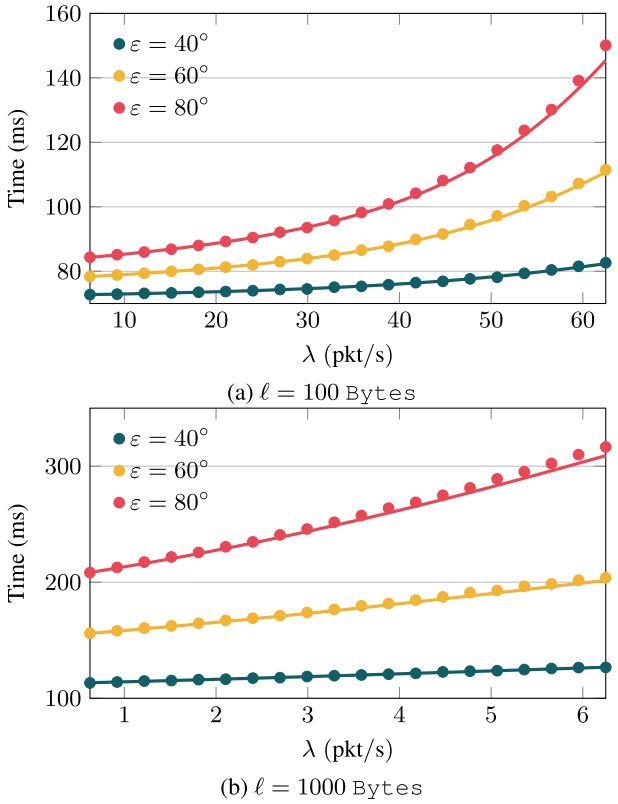

FIGURE 9. Average end-to-end total delay vs. packet arrival rate for different average packet lengths. Theoretical and simulated values are shown with solid lines and markers, respectively.

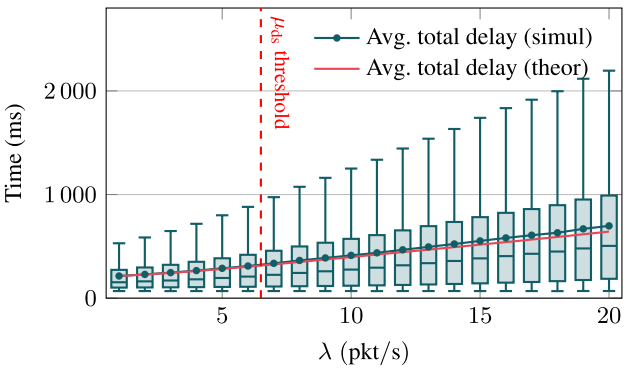

FIGURE 10. Box-and-whisker plot of delay distribution for elevation $\varepsilon = 80°$ and average packet length $\ell = 1000$ `Bytes`. The results are obtained from a single simulation where 10^6 packets are transmitted trough the chain of satellites. Theoretical and simulated average values are depicted with solid lines and markers, respectively.

3) EFFECT OF TRAFFIC PATTERN DISTRIBUTIONS

We can also exploit the simulator to assess the performance without the assumptions that were previously made regarding incoming traffic and packet length distributions (Poisson and exponential, respectively). Figure 11 uses a box-and-whisker plot to show how the end-to-end delay was distributed for three different cases: the green boxes correspond to the results discussed above, where the incoming traffic was Poisson, and packet length was exponentially distributed. Yellow boxes show the results obtained when the packet length was constant, equal to the average value used earlier, and the traffic pattern was not changed. Last, the red boxes reflect the values obtained when both the traffic rate and the packet length were constant. As can be seen, there is not a relevant difference between the first two configurations. However, when the traffic rate was constant, the results yield a lower average delay, which also showed less dispersion. In any case, the results obtained with the proposed model would yield a good indication of the expected performance, regardless of the particular distributions used for the incoming traffic process and the packet lengths.

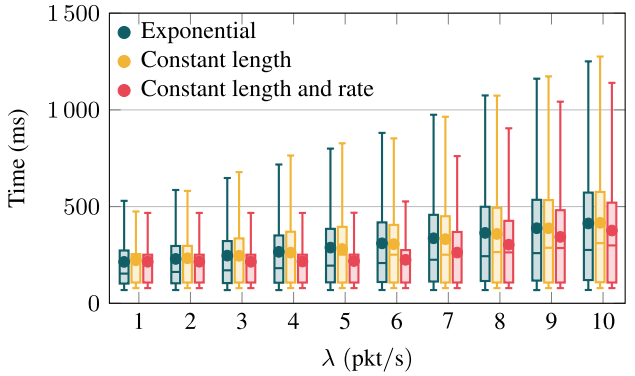

FIGURE 11. Box-and-whisker plot of total delay distribution for $\varepsilon = 80°$ and different packet length and incoming traffic distributions with $\ell = 1000$ Bytes.

C. IMPACT OF BACKGROUND TRAFFIC

In this section we broaden the complexity of the scenario. We assume that there might be some ISLs used by other communication paths, and we thus increase the occupancy of such links. This in turn might impact the end-to-end delay on the original traffic flow of interest, which is the same as we studied previously. Hence, by using the same baseline setup, we assume that there exists background traffic in a number of ISL, each with rate γ. We fix the rate of the traffic of interest to 0.5 μ_{ds}. In addition, γ is selected so that the capacity of the k^{th} ISL, $(\mu_{\text{mm1}})_k$, is not exceeded by the aggregated traffic, i.e. $(\rho_{\text{mm1}})_k \leq 1 \; \forall k = 1 \ldots K-1$. In all cases a packet length of 1000 Bytes is used.

First, Figure 12 compares the results that were obtained with the proposed theoretical model with the performance that was observed using the simulator, when $\gamma \in \{0.5\ \mu_{\text{mm1}}, 0.9\ \mu_{\text{mm1}}\}$. We added such background traffic in 1 and 4 ISLs. Again, we can see a good match between

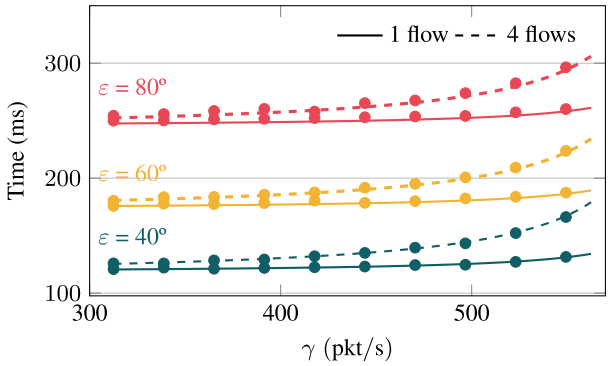

FIGURE 12. End-to-end traffic delay vs. background traffic for $\ell = 1000$ Bytes. Theoretical and simulated results are shown with lines and markers, respectively. For each elevation configuration results are shown for 1 and 4 background flows with solid and dashed lines, respectively.

analytical and real performances (the ones observed with the simulator). The results evince the impact of sharing the capacities of the intermediate nodes with other traffic flows. This might jeopardize the end-to-end delay, especially when there are more links with background traffic, and the total is close to their capacity. On the other hand, if the number of links with background traffic is low, the impact of increasing such traffic over the end-to-end delay is not that relevant.

More interestingly, Figure 13 shows the variability of such end-to-end delay for a number of configurations considering background traffic. There are three groups of boxplots (left-side) for the configuration with just 1 background traffic flow, and another three for the results obtained with 4 flows, one per elevation value. In each of these groups, we have three values of γ, increasing the corresponding link occupancy. The results evince that the variability of the end-to-end delay is mostly due to the behavior of the LMS links, and in particular to the elevation configuration. In this sense, for the experiments having 1 single background traffic flow, the increase of both the average delay and its variability is almost negligible. When there are four links having background traffic, and they are close to their maximum capacity ($\gamma = 0.9\ \mu_{\text{mm1}}$), there is a more noticeable increase, which is more relevant for

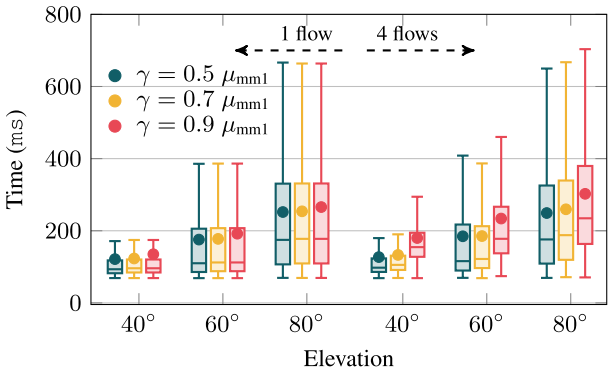

FIGURE 13. Box-and-whisker plots of the end-to-end delay when there is background traffic with $\ell = 1000$ Bytes. Average values are shown with markers within each of the boxes.

the 40° configuration of the LMS links, since their delay was significantly lower.

VI. CONCLUSION

In this paper we propose a novel queuing model that can be used to study the end-to-end delay in LEO satellite constellations. It considers a communication path between two ground stations connected through a chain of inter-satellite links. The first and last LMS links (those with the connected ground stations) are modeled with a novel two dimensional Markov chain that captures the evolution of the corresponding channel conditions and queued packets, while a stable ISL is modeled by a classical $M/M/1$ queuing system. The validity of the proposed model solved with the Matrix Geometric Method, has been assessed by means of an ad-hoc event-driven simulator. This has been later exploited to broaden the analysis, considering not only the average performance, but also the delay variability total end-to-end delay, background traffic of other distinct traffic flows, and traffic pattern distributions, since it might have a relevant impact on certain real-time IoT-based services.

The obtained results show a very good match between the proposed model and system simulations in all evaluated scenarios. It highlights the importance of proper modeling and capturing the different channel states in the queuing delay. Depending on these particular characteristics, packet queues can be kept relatively low, while the end-to-end delay might suffer from an important variability. On the other hand, the impact of the intermediate nodes (provided they can ensure a good channel condition) is much less relevant, though the background traffic is significant as the number of flows or their rate increases. Similarly, it was corroborated that differences between a Poissonian distribution and others for the total aggregated traffic is not significant. In our future work, we will exploit both the proposed model and the developed simulator to increase the complexity of the scenario. We will consider finite buffer lengths, which might cause packets to be discarded, as well as erasure events to study the trade-off between delay and loss probability. We will also assess its feasibility with other constellation heights, for instance MEO. In addition, we will investigate different queuing policies and QoS mechanisms, which might, for instance, apply various priority levels to control and payload traffics in IoT services.

REFERENCES

[1] NewSpace Global LLC. (2021). *NSG: Global Leader in Data Analysis and Coverage of the NewSpace Industry*. [Online]. Available: https://newspaceglobal.com/

[2] European Space Agency. (2016). *What is space 4.0*. [Online]. Available: http://www.esa.int/About_Us/Ministerial_Council_2016/What_is_space_4.0

[3] Erik Kulu. (2016). *NewSpace Index: Overview of Costellations, Launchers and Funding*. [Online]. Available: https://www.newspace.im/

[4] National Aeronautics and Space Administration (NASA). (2020). *ARTEMIS: Humanity's Return to the Moon*. [Online]. Available: https://www.nasa.gov/specials/artemis/

[5] SpaceX. (2020). *Company Website*. [Online]. Available: https://www.spacex.com/

[6] Blue Origin. (2020). *Company Website*. [Online]. Available: https://www.blueorigin.com/

[7] (2020). *CubeSat Design Specification. Revision 14*. [Online]. Available: https://www.cubesat.org/cds-announcement

[8] (Mar. 31, 2018). *Nanosat Public Database From EU-FP7 NANOSAT*. Accessed: Nov. 1, 2018. [Online]. Available: http://nanosats.eu/

[9] P. Wang, J. Zhang, X. Zhang, Z. Yan, B. G. Evans, and W. Wang, "Convergence of satellite and terrestrial networks: A comprehensive survey," *IEEE Access*, vol. 8, pp. 5550–5588, 2020.

[10] *Study on New Radio (NR) to Support Non-Terrestrial Networks*, Standard TR 38.811 V15.1.0, 3GPP, Tech. Rep., Jun. 2019.

[11] F. Lázaro, R. Raulefs, W. Wang, F. Clazzer, and S. Plass, "VHF data exchange system (VDES): An enabling technology for maritime communications," *CEAS Space J.*, vol. 11, no. 1, pp. 55–63, Mar. 2019.

[12] *Satellite Detection of Automatic Identification System Messages*, document ITU, ITU-R M.2014ITU-R, Tech. Rep., 2006.

[13] T. C. Smith, "Automatic dependent surveillance broadcast (ADS-B) out performance requirements to support air traffic control (ATC) service, final rules," FAA, Federal Aviation Admin., Washington, DC, USA, Tech. Rep., FAA, Rule 14 CFRPart 91, 2010.

[14] L. Kleinrock, *Queueing Systems: Theory*, vol. 1. Hoboken, NJ, USA: Wiley, 1975.

[15] F. P. Kelly, "Networks of queues," *Adv. Appl. Probab.*, vol. 8, no. 2, pp. 416–432, 1976.

[16] P. J. Burke, "The output of a queuing system," *Oper. Res.*, vol. 4, no. 6, pp. 699–704, Dec. 1956.

[17] J. R. Jackson, "Jobshop-like queueing systems," *Manage. Sci.*, vol. 50, no. 12, pp. 1796–1802, Dec. 2004.

[18] F. P. Fontan, M. Vazquez-Castro, C. E. Cabado, J. P. Garcia, and E. Kubista, "Statistical modeling of the LMS channel," *IEEE Trans. Veh. Technol.*, vol. 50, no. 6, pp. 1549–1567, Nov. 2001.

[19] A. Chen, C.-T. Chang, and Y.-D. Yao, "Performance evaluation of ARQ operations with OBP and inter-satellite links: Delay performance," in *Proc. IEEE 54th Veh. Technol. Conf. (VTC Fall)*, Oct. 2001, pp. 2346–2350.

[20] B. S. Yeo, "An average end-to-end packet delay analysis for LEO satellite networks," in *Proc. IEEE 56th Veh. Technol. Conf.*, Sep. 2002, pp. 2012–2016.

[21] R. Hermenier, C. Kissling, and A. Donner, "A delay model for satellite constellation networks with inter-satellite links," in *Proc. Int. Workshop Satell. Space Commun.*, Sep. 2009, pp. 3–7.

[22] L. Tan, Y. Liu, and J. Ma, "Analysis of queuing delay in optical space network on LEO satellite constellations," *Optik*, vol. 125, no. 3, pp. 1154–1157, Feb. 2014.

[23] T. Li, H. Zhou, H. Luo, W. Quan, and S. Yu, "Modeling software defined satellite networks using queueing theory," in *Proc. IEEE Int. Conf. Commun. (ICC)*, May 2017, pp. 1–6.

[24] Y. Zhu, L. Qian, L. Ding, F. Yang, C. Zhi, and T. Song, "Software defined routing algorithm in LEO satellite networks," in *Proc. Int. Conf. Electr. Eng. Informat. (ICELTICs)*, Oct. 2017, pp. 257–262.

[25] Y. Zhu, M. Sheng, J. Li, and R. Liu, "Performance analysis of intermittent satellite links with time-limited queuing model," *IEEE Commun. Lett.*, vol. 22, no. 11, pp. 2282–2285, Nov. 2018.

[26] U. Speidel and L. Qian, "Striking a balance between bufferbloat and TCP queue oscillation in satellite input buffers," in *Proc. IEEE Global Commun. Conf. (GLOBECOM)*, Dec. 2018, pp. 1–6.

[27] H. Li, H. Zhang, L. Qiao, F. Tang, W. Xu, L. Chen, and J. Li, "Queue state based dynamical routing for non-geostationary satellite networks," in *Proc. IEEE 32nd Int. Conf. Adv. Inf. Netw. Appl. (AINA)*, May 2018, pp. 1–8.

[28] Y. Nie, Z. Fang, and S. Gao, "Survivability analysis of LEO satellite networks based on network utility," *IEEE Access*, vol. 7, pp. 123182–123194, 2019.

[29] B. Soret, S. Ravikanti, and P. Popovski, "Latency and timeliness in multi-hop satellite networks," in *Proc. IEEE Int. Conf. Commun. (ICC)*, Jun. 2020, pp. 1–6.

[30] B. Soret, I. Leyva-Mayorga, S. Cioni, and P. Popovski, "5G satellite networks for Internet of Things: Offloading and backhauling," *Int. J. Satell. Commun. Netw.*, vol. 39, no. 4, pp. 431–444, 2021. [Online]. Available: https://www.onlinelibrary.wiley.com/doi/abs/10.1002/sat.1394, doi: 10.1002/sat.1394.

[31] F. Chiariotti, O. Vikhrova, B. Soret, and P. Popovski, "Information freshness of updates sent over LEO satellite multi-hop networks," 2020, *arXiv:2007.05449*. [Online]. Available: https://arxiv.org/abs/2007.05449

[32] J. R. Wertz and W. J. Larson, *Space Mission Analysis and Design*, 3rd ed. Norwell, MA, USA: Kluwer, 1999.
[33] D. Beste, "Design of satellite constellations for optimal continuous coverage," *IEEE Trans. Aerosp. Electron. Syst.*, vol. AES-14, no. 3, pp. 466–473, May 1978.
[34] F. Metzger, T. Hobfeld, A. Bauer, S. Kounev, and P. E. Heegaard, "Modeling of aggregated IoT traffic and its application to an IoT cloud," *Proc. IEEE*, vol. 107, no. 4, pp. 679–694, Apr. 2019.
[35] M. F. Neuts, "Markov chains with applications in queueing theory, which have a matrix-geometric invariant probability vector," *Adv. Appl. Probab.*, vol. 10, no. 1, pp. 185–212, Mar. 1978.
[36] B. Hajek, "Birth-and-death processes on the integers with phases and general boundaries," *J. Appl. Probab.*, vol. 19, no. 3, pp. 488–499, 1982.
[37] M. Neuts, *Matrix-Geometric Solutions Stochastic Models: An Algorithmic Approach*. Baltimore, MD, USA: Johns Hopkins Univ. Press, 1981.
[38] F. Malandra, L. O. Chiquette, L.-P. Lafontaine-Bédard, and B. Sansò, "Traffic characterization and LTE performance analysis for M2M communications in smart cities," *Pervas. Mobile Comput.*, vol. 48, pp. 59–68, Aug. 2018. [Online]. Available: http://www.sciencedirect.com/science/article/pii/S1574119217306089

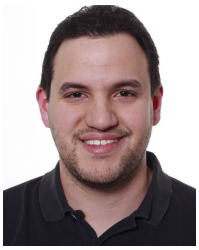

NÉSTOR J. HERNÁNDEZ MARCANO (Member, IEEE) received the M.Sc. degree in electronics engineering, digital communications from Universidad Simón Bolívar, Venezuela, in 2013, and the Ph.D. degree in wireless communications from Aalborg University, in 2016. He has been a Postdoctoral Researcher with the Network and Analytics (NAN) Group, Department of Electrical and Computer Engineering, Aarhus University, since 2017. His research interests include wireless communications systems and networks, error/erasure correcting codes, space-ground integrated networks, and network security. He is a part of the Aarhus Space Center initiative at Aarhus University focusing on small- and micro-satellite missions for astronomical and engineering applications. He served as a TPC member for the ICC 2021 Workshop in Satellite Mega-Constellations in the 6G Era (6GSatComNet). He is a Reviewer of VTC, ICC, and GLOBECOM.

LUIS DIEZ received the M.Sc. and Ph.D. degrees from the University of Cantabria, in 2013 and 2018, respectively. He is currently an Assistant Professor with the Communications Engineering Department, University of Cantabria. He has been involved in different international and industrial research projects. His research interests include future network architectures, resource management in wireless heterogeneous networks, and the IoT solutions and services. He has published more than 40 scientific and technical articles in those areas. He has served as a TPC member and a reviewer in a number of international conferences and journals. As for teaching, he has supervised 15 B.Sc. and M.Sc. theses. He teaches in courses related to cellular networks, network dimensioning, and service management.

RAMÓN AGÜERO CALVO (Senior Member, IEEE) received the M.Sc. degree (Hons.) in telecommunications engineering from the University of Cantabria, in 2001, and the Ph.D. degree (Hons.), in 2008. Since 2016, he has been the Head of the IT area (deputy CIO) at the University of Cantabria. He is currently an Associate Professor with the Communications Engineering Department, University of Cantabria. His research interests include future network architectures, especially regarding the (wireless) access part of the network and its management. He is interested on multihop (mesh) networks and network coding. He has published more than 200 scientific articles in such areas. He has supervised five Ph.D. students and more than 70 B.Sc. and M.Sc. theses. He is the main instructor in courses dealing with networks and traffic modeling at B.Sc. and M.Sc. levels. He is a regular TPC member and a reviewer on various related conferences and journals. He has been serving in the Editorial Board of IEEE Communication Letters as a Senior Editor, since 2019. He serves in the Editorial Board of IEEE Open Access Journal of the Communications Society, *Wireless Networks* (Springer), and *Mobile Information Systems* (Hindawi).

RUNE HYLSBERG JACOBSEN (Senior Member, IEEE) received the master's degree in science in physics and chemistry from Aarhus University, Denmark, and the Ph.D. degree in laser physics and optoelectronics from Aarhus University, in 1997. He is currently an Associate Professor with the Department of Electrical and Computer Engineering, Aarhus University. His primary research interests include computer networking, wireless communications, network security, data analytics, cooperative intelligent systems, and nanosatellite communications. His professional career spans more than 14 years in the telecommunications and IT industry, where he has been responsible for the management of research and development. He has published more than 85 peer-reviewed journal and conference papers in areas of communications and its applications.